

Characterization of magnetic CoFe cyanides by x-ray-absorption fine-structure spectroscopy

Toshihiko Yokoyama and Toshiaki Ohta

Department of Chemistry, Graduate School of Science, The University of Tokyo, 7-3-1 Hongo, Bunkyo-ku, Tokyo 113-0033, Japan

Osamu Sato

Kanagawa Academy of Science and Technology, Tokyo Institute of Polytechnics, 1583 Iiyama, Atsugi, Kanagawa 243-0213, Japan

Kazuhito Hashimoto

*Kanagawa Academy of Science and Technology, Tokyo Institute of Polytechnics, 1583 Iiyama, Atsugi, Kanagawa 243-0213, Japan
and Research Center for Advanced Science and Technology, The University of Tokyo, 4-6-1 Komaba, Meguro-ku, Tokyo 153-0041, Japan*

(Received 28 April 1998)

X-ray-absorption fine-structure spectra were measured and analyzed for several FeCo cyanides $M_x\text{Co}_y\text{Fe}(\text{CN})_6 \cdot z\text{H}_2\text{O}$ ($M = \text{Na}, \text{K}, \text{Rb}$) which are known to exhibit interesting magnetic properties depending on temperature. X-ray-absorption near-edge structure spectra allow us to confirm very clearly the spin transitions in $\text{Na}_{0.4}\text{Co}_{1.3}\text{Fe}(\text{CN})_6 \cdot 5\text{H}_2\text{O}$ and $\text{K}_{0.4}\text{Co}_{1.3}\text{Fe}(\text{CN})_6 \cdot 5\text{H}_2\text{O}$ and to evaluate the composition ratios of Co^{II} and Co^{III} species quantitatively. The $\text{Co}^{\text{II}}:\text{Co}^{\text{III}}$ ratios are essentially important physical quantities with which to understand magnetic properties. The local structures around Fe and Co atoms were determined by the Fe and Co K -edge extended x-ray-absorption fine-structure spectra. It is confirmed that the local structures around Fe are $\text{Fe}(\text{CN})_6\text{Co}_6$ (the subscripts denote the coordination numbers) while those around Co are $\text{Co}(\text{NC})_{6-1/y}(\text{H}_2\text{O})_{1/y}\text{Fe}_{6-1/y}$. The first-nearest-neighbor Fe-C distances do not significantly change between Fe^{II} and Fe^{III} species, while the first-nearest-neighbor Co-NO distances are noticeably different between Co^{II} and Co^{III} ones. The difference of as much as 0.16–0.20 Å between Co^{II} and Co^{III} , which corresponds well to that for typical Co tautomeric complexes, causes noticeable change of the lattice constant.

[S0163-1829(98)00138-6]

I. INTRODUCTION

Prussian blue analogs have recently attracted great interest because of their various characteristics as molecular magnets. High critical temperatures (T_c) have been reported by several research groups.^{1–4} Ferlay *et al.*³ reported $T_c = 315$ K for $\text{V}[\text{Cr}(\text{CN})_6]_{0.86} \cdot 2.8\text{H}_2\text{O}$ (air sensitive), while Sato *et al.*⁴ obtained $T_c = 270$ K for $\text{Cr}_{2.12}(\text{CN})_6$ (air stable). These T_c values are in the highest T_c region among molecule-based magnets that have ever been prepared to date. On the other hand, Sato *et al.*⁵ discovered the induction of a magnetic phase transition by optical stimuli. They clarified that in $\text{K}_{0.2}\text{Co}_{1.4}[\text{Fe}(\text{CN})_6] \cdot 6.9\text{H}_2\text{O}$ the ferrimagnetic regions are substantially extended after red-light illumination is restored to the original level upon heating. Moreover, Ohkoshi *et al.*⁶ succeeded in controlling the saturation magnetization, the Weiss temperatures, and the coercive fields in ferromagnets and ferrimagnets $(\text{Ni}_x\text{Mn}_{1-x})_{1.5}[\text{Cr}(\text{CN})_6]$ by varying x . These various kinds of important observations are owing to easy modification of the materials by changing the composition ratios of various transition metal cations such as V, Cr, Mn, Fe, Co, and Ni.

Although structural information on these Prussian blue analogs is quite important to the understanding of observed magnetic properties and to the design of new magnetic materials, the single-crystal x-ray-diffraction technique is hardly applicable since these materials can usually be obtained only as fine powder. Prussian blue $\text{Fe}_4^{\text{III}}[\text{Fe}^{\text{II}}(\text{CN})_6]_3 \cdot 15\text{H}_2\text{O}$ itself

is one of a few examples that have been investigated by x-ray crystallography so far, though great efforts were required for the growth of single crystals.⁷ No structure determination has been performed for recently synthesized materials. In these materials, long-range structure can be expected as an analog to Prussian blue, while the local structure is still unknown, which plays a significant role in the magnetic properties. In such a case, extended x-ray-absorption fine-structure (EXAFS) spectroscopy⁸ is useful to reveal local structures around transition-metal atoms. The EXAFS spectroscopy allows us to obtain information on coordination numbers and interatomic distances around the x-ray-absorbing atoms. Moreover, electronic properties can simultaneously be studied by the measurements of x-ray-absorption near-edge structure (XANES) spectra.⁸

In the present study, we have measured and analyzed the Fe and Co K -edge XAFS (x-ray-absorption fine-structure) spectra of several CoFe cyanides.⁹ In this group, the Co and Fe valences are known to vary, depending on the compositions, the kinds of alkali ions, temperature, etc. Moreover, mixed valences are expected especially for Co ions. The changes of local structures are thus one of the main subjects in the present investigation. The relationship between the Fe/Co valences and the local structure will quantitatively be clarified. The other subject is to reveal quantitatively the composition ratios such as $\text{Co}^{\text{II}}:\text{Co}^{\text{III}}$ in each material from the XANES spectra. This information is substantially important, not only to the understanding of the magnetic properties

TABLE I. List of the samples investigated. The fcc lattice constants a_0 at room temperature and expected local structures around Co are also given. Local structures around Fe may be $\text{Fe}(\text{CN})_6\text{Co}_6$ for all the samples.

Sample	Composition	Synthesis method	a_0 (Å)	Local structure around Co
(a)	$\text{Rb}_{0.66}\text{Co}_{1.25}\text{Fe}(\text{CN})_6 \cdot 4.3\text{H}_2\text{O}$	Solution mixing	9.96	$\text{Co}(\text{NC})_{4.80}(\text{H}_2\text{O})_{1.20}\text{Fe}_{4.80}$
(b)	$\text{K}_{0.4}\text{Co}_{1.3}\text{Fe}(\text{CN})_6 \cdot 5\text{H}_2\text{O}$	Electrochemical	9.96	$\text{Co}(\text{NC})_{4.61}(\text{H}_2\text{O})_{1.39}\text{Fe}_{4.61}$
(c)	$\text{Na}_{0.4}\text{Co}_{1.3}\text{Fe}(\text{CN})_6 \cdot 5\text{H}_2\text{O}$	Electrochemical	10.33	$\text{Co}(\text{NC})_{4.61}(\text{H}_2\text{O})_{1.39}\text{Fe}_{4.61}$
(d)	$\text{K}_{0.4}\text{Co}_{1.3}\text{Fe}(\text{CN})_6 \cdot 4.2\text{H}_2\text{O}$	Solution mixing	10.30	$\text{Co}(\text{NC})_{4.61}(\text{H}_2\text{O})_{1.39}\text{Fe}_{4.61}$
(e)	$\text{Na}_{1.4}\text{Co}_{1.3}\text{Fe}(\text{CN})_6 \cdot 5\text{H}_2\text{O}$	Electrochemical	10.31	$\text{Co}(\text{NC})_{4.61}(\text{H}_2\text{O})_{1.39}\text{Fe}_{4.61}$
(f)	$\text{Co}_{1.5}\text{Fe}(\text{CN})_6 \cdot 6\text{H}_2\text{O}$	Solution mixing	10.32	$\text{Co}(\text{NC})_{4.00}(\text{H}_2\text{O})_{2.00}\text{Fe}_{4.00}$

because of direct participation of the Co 3d electrons in magnetism, but also to the ability to perform reliable EXAFS analyses since the $\text{Co}^{\text{II}}:\text{Co}^{\text{III}}$ composition ratios cannot be estimated by EXAFS itself because of too many unknown variables. As shown below, with the Co *K*-edge XANES spectra we have been able to determine the composition ratios by comparing several kinds of the spectra. The present analytical procedures are also useful in a methodological sense.

II. MATERIALS

Detailed preparation procedures of the materials investigated are described elsewhere.^{9,10} A list of the materials is summarized in Table I. Briefly, samples (b), (c), and (e) were synthesized electrochemically, while (a), (d), and (f) were produced by simply mixing aqueous solutions. The fcc lattice constants a_0 are also noted in Table I. Sample (a) contains Rb^+ and shows no magnetic transition. Sample (b) containing K^+ exhibits a change from the paramagnetic phase to the ferrimagnetic one ($T_c = 26$ K) upon irradiation of visible lights. In sample (c), K^+ is replaced with Na^+ and a charge-transfer transition occurs below 260 K from $\text{Fe}^{\text{III}}\text{-CN-Co}^{\text{II}}$ to $\text{Fe}^{\text{II}}\text{-CN-Co}^{\text{III}}$, where Co^{II} and Co^{III} give, respectively, high-spin ($S = \frac{3}{2}$) and low-spin ($S = 0$) states. Sample (d) shows a similar spin transition around 280 K. In samples (e) and (f), Co atoms are (almost) always divalent.

All the present materials are regarded as a Prussian blue analog, the structure of which is schematically shown in Fig. 1. This structure was clarified by the single-crystal x-ray-diffraction analysis of Prussian blue $\text{Fe}_4^{\text{III}}[\text{Fe}^{\text{II}}(\text{CN})_6]_3 \cdot 15\text{H}_2\text{O}$.⁷ In $\text{Fe}_4^{\text{III}}[\text{Fe}^{\text{II}}(\text{CN})_6]_3 \cdot 15\text{H}_2\text{O}$, only $\frac{3}{4}$ of the $\text{Fe}^{\text{II}}(\text{CN})_6$ site is occupied and there exist randomly distributed defects of the $\text{Fe}^{\text{II}}(\text{CN})_6$ unit. Thus the average local structure around Fe^{II} is simply given as $\text{Fe}^{\text{II}}(\text{CN})_6\text{Fe}_6^{\text{III}}$ (subscript numbers denote coordination numbers), while the one around Fe^{III} should be $\text{Fe}^{\text{III}}(\text{NC})_{4.5}(\text{H}_2\text{O})_{1.5}\text{Fe}_4^{\text{II}}$ as a result of the H_2O coordination instead of NC^- . In $\text{Fe}_4^{\text{III}}[\text{Fe}^{\text{II}}(\text{CN})_6]_3 \cdot 15\text{H}_2\text{O}$ ($a_0 = 10.166$ Å), the $\text{Fe}^{\text{II}}\text{-C}$, C-N , and $\text{Fe}^{\text{III}}\text{-N}$ distances were given as 1.92, 1.13, and 2.03 Å, respectively. In all the present materials, the average local structures around Fe are similarly expected to be $\text{Fe}(\text{CN})_6\text{Co}_6$. Those around Co are considered from the Fe:Co composition ratios as given in Table I.

III. XAFS MEASUREMENTS

Fe and Co *K*-edge XAFS spectra were taken in the conventional transmission mode at the Beamline 7C of the Pho-

ton Factory (operation energy of 2.5 GeV and stored current of 400–200 mA) at the Institute of Materials Structure Science.¹¹ Si(111) double crystals (the first crystal was cooled with water) were employed as a monochromator without focusing. In order to reduce higher-order harmonics, the double crystals were detuned around $\sim 60\%$. No mirrors were inserted in the present setup. The intensities of the incident and transmitted x rays were recorded using ionization chambers filled with pure N_2 . Although the absolute photon energy was not calibrated, the relative photon energies never changed during the measurements within the employed energy step (0.2 eV), judging from several glitches appearing in the I_0 function. The samples were diluted with BN to give pellets with appropriate thickness. The edge jumps were found to be around 0.3–0.5 for Fe and Co *K* edges for all the samples, and the total absorption coefficients were estimated to be at most 2.0. The spectra were measured at 30 and 296 K. For reference, Fe *K*-edge XAFS of $\text{K}_3\text{Fe}^{\text{III}}(\text{CN})_6$, $\text{K}_4\text{Fe}^{\text{II}}(\text{CN})_6 \cdot 3\text{H}_2\text{O}$ and Co *K*-edge XAFS of $\text{Co}^{\text{II}}(\text{NO}_3)_2$ hydrate and $\text{K}_3\text{Co}^{\text{III}}(\text{CN})_6$ were taken at 296 K.

Fe *K*-edge EXAFS is recorded only up to $k \sim 12.3$ Å⁻¹ (k is the photoelectron wave number) because of the presence of Co. On the other hand, Co *K*-edge EXAFS could be taken with wider energy ranges. A trace amount of Ni impurities ($\sim 0.1\%$ of Co) was, however, found for all the materials, this limiting the k range up to ~ 12.5 Å⁻¹.

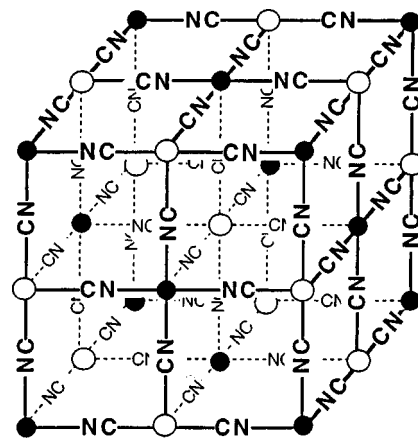


FIG. 1. Schematic view of the structure of the CoFe cyanide (○, Fe; ●, Co). The $\text{Fe}(\text{CN})_6$ unit is only partly occupied. The Co ions next to the $\text{Fe}(\text{CN})_6$ lack may be coordinated by H_2O instead of NC^- .

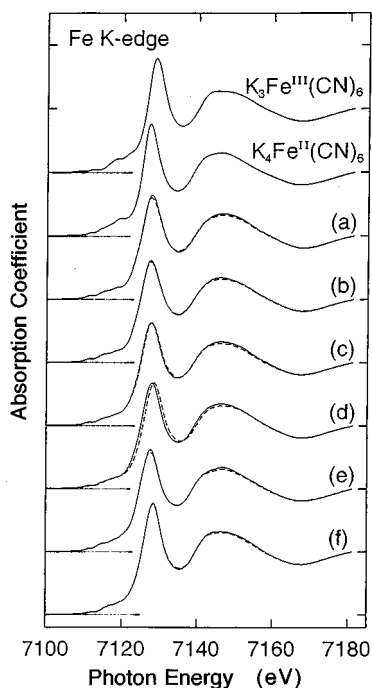


FIG. 2. Fe *K*-edge XANES spectra (7100–7180 eV) of samples (a)–(f) taken at 30 K (solid lines) and 296 K (dashed lines). Those of $\text{K}_3\text{Fe}^{\text{III}}(\text{CN})_6$ and $\text{K}_4\text{Fe}^{\text{II}}(\text{CN})_6 \cdot 3\text{H}_2\text{O}$ at 296 K are also depicted as references.

IV. XANES

A. Fe *K*-edge XANES

Figure 2 shows the Fe *K*-edge XANES spectra of samples (a)–(f), $\text{K}_3\text{Fe}^{\text{III}}(\text{CN})_6$ and $\text{K}_4\text{Fe}^{\text{II}}(\text{CN})_6$. All the spectra resemble each other, indicatively confirming that the local structure of Fe is $\text{Fe}(\text{CN})_6$. Slight differences are nevertheless found between $\text{K}_3\text{Fe}^{\text{III}}(\text{CN})_6$ and $\text{K}_4\text{Fe}^{\text{II}}(\text{CN})_6$. The spectral features of sample (e) are closer to $\text{K}_4\text{Fe}^{\text{II}}(\text{CN})_6$ than to $\text{K}_3\text{Fe}^{\text{III}}(\text{CN})_6$, implying divalent Fe at both 30 and 296 K. On the contrary, those of sample (f) resemble $\text{K}_3\text{Fe}^{\text{III}}(\text{CN})_6$ more closely, suggesting trivalent Fe. Sample (d) shows clear temperature dependence of the edge energy, indicating the charge-transfer transition between Fe^{II} and Fe^{III} .

Figure 3 shows the pre-edge regions of the Fe *K*-edge XANES spectra. The peaks at ~ 7108 and ~ 7112 eV in $\text{K}_3\text{Fe}^{\text{III}}(\text{CN})_6$ can be attributed to the transitions of $\text{Fe } 1s \rightarrow 3dt_{2g}$ and $\text{Fe } 1s \rightarrow 3de_g$, respectively, while the one at ~ 7111 eV in $\text{KFe}^{\text{II}}(\text{CN})_6$ corresponds to the $\text{Fe } 1s \rightarrow 3de_g$ transition and no $\text{Fe } 1s \rightarrow 3dt_{2g}$ transition can be found in $\text{KFe}^{\text{II}}(\text{CN})_6$ because of complete occupation of the Fe $3dt_{2g}$ levels.¹² Using these features, samples (a), (b), and (e) are found to consist of Fe^{II} , while sample (f) contains Fe^{III} . Spectra (c) and (d) exhibit temperature dependence, supporting the charge-transfer transitions.

Although some differences were observed in the Fe *K*-edge XANES spectra including temperature dependence, overall features resemble each other closely and no quantitative analysis of the XANES spectra could be performed to elucidate the concentrations of Fe^{II} and Fe^{III} species. A principal conclusion might be that the local structures of Fe were confirmed to be $\text{Fe}(\text{CN})_6$ for all the materials.

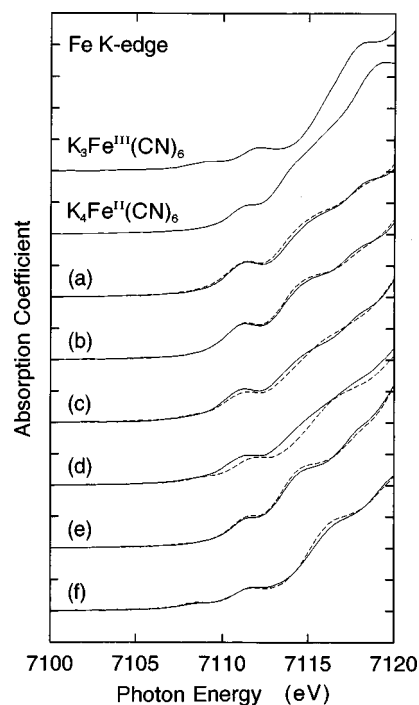


FIG. 3. Expanded Fe *K*-edge XANES spectra (7100–7120 eV) of samples (a)–(f) taken at 30 K (solid lines) and 296 K (dashed lines). Those of $\text{K}_3\text{Fe}^{\text{III}}(\text{CN})_6$ and $\text{K}_4\text{Fe}^{\text{II}}(\text{CN})_6 \cdot 3\text{H}_2\text{O}$ at 296 K are also depicted as references.

B. Co *K*-edge XANES

Co *K*-edge XANES spectra are shown in Fig. 4. Much clearer differences can be found among the spectra. The spectral features of samples (a), (b), (e), and (f) show less temperature dependence, while those of samples (c) and (d) exemplify noticeable differences between 30 and 296 K. The

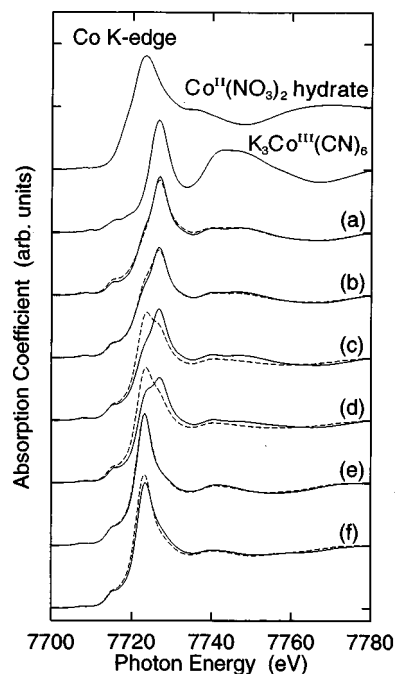


FIG. 4. Co *K*-edge XANES spectra of samples (a)–(f) taken at 30 K (solid lines) and 296 K (dashed lines). Those of $\text{K}_3\text{Co}^{\text{III}}(\text{CN})_6$ and $\text{Co}(\text{NO}_3)_2$ hydrate at 296 K are also depicted as references.

spectra of samples (e) and (f) composed of Co^{II} give intense resonances at ~ 7723 eV, while those of samples (a) and (b) that contain mainly Co^{III} rather than Co^{II} show similar resonances at ~ 7727 eV. The temperature differences seen in samples (c) and (d) indicate the transition between Co^{III} and Co^{II} . It should be, however, noted that significant amounts of Co^{III} still exist at 296 K.

It seems that the spectra of samples (a)–(d) can be expressed as a sum of the spectra of pure Co^{II} and Co^{III} species. This is reasonable since the local structures around Co are quite similar among the materials $[\text{Co}(\text{NC})_{4.8}(\text{H}_2\text{O})_{1.2}\text{Fe}_{4.8}]$ for sample (a), $\text{Co}(\text{NC})_{4.61}(\text{H}_2\text{O})_{1.39}\text{Fe}_{4.61}$ for samples (b)–(e), and $\text{Co}(\text{NC})_{4.0}(\text{H}_2\text{O})_{2.0}\text{Fe}_{4.0}$ for sample (f)]. In the case of many independent ensembles available, the statistical factor analysis can, in principle, be performed to obtain the number of components, the spectrum of each component, and the composition ratio of each component in the ensemble.¹³ In the present case, the analysis seems rather easy since the pure Co^{II} spectrum is (almost) known as the one of samples (e) and (f). Although the factor analysis requires very accurate energy calibration, no energy shifts beyond the employed energy step (0.2 eV) were observed in the present measurements, which was verified by the energy positions of several monochromator glitches. Thus no artificial energy correction is needed in the present analysis.

Since the local structure of sample (f) is a little different from the others, ten spectra of samples (a)–(e) were at first employed to obtain the eigenvalues of the covariance matrix. These were 1.95×10^3 , 1.93×10 , 2.17×10^{-1} , 5.92×10^{-2} , 3.41×10^{-2} , ..., which proved that the number of the components is two, namely, Co^{II} and Co^{III} components. The results did not meaningfully change when sample (f) was also included in the analysis. Through the data handling, it was found to be most reliable to assume that the spectrum of sample (e) at 296 K is described with only the pure Co^{II} spectrum. This assumption is quite reasonable from the chemical composition. The pure Co^{III} spectrum and the $\text{Co}^{\text{II}}:\text{Co}^{\text{III}}$ composition ratio in each sample can thus be obtained using a standard linear least-squares fitting.

The examples of the analysis results are depicted in Fig. 5 and the Co^{III} composition ratios are tabulated in Table II. It is not so easy to estimate the errors in the obtained values because there exist several nonstatistical error origins such as the normalization process of the XANES spectra and the assumption that Co^{II} and Co^{III} components, respectively, show exactly the same features in all the spectra. Nevertheless, when the component ratio varies by a few percent, the corresponding sum spectrum was found to change noticeably. We can thus expect that the accuracy is within a few percent in the present analysis. In samples (a), (b) and (e), less temperature dependence concerning the $\text{Co}^{\text{II}}/\text{Co}^{\text{III}}$ composition ratios is found, while in samples (c) and (d) charge transfer is quantitatively clarified between 30 and 296 K. It should be also noted that, although the analysis of sample (f) is less reliable because of somewhat different local structure from the others, a slight increase in the Co^{III} ratio with the temperature decrease is seen, indicating a small amount of charge transfer between Fe^{III} and Co^{II} at low temperature. Actually, as given in the Fe K -edge XANES of Fig. 2, the Fe $1s \rightarrow 3dt_{2g}$ transition intensity is slightly reduced from 296 to 30 K.

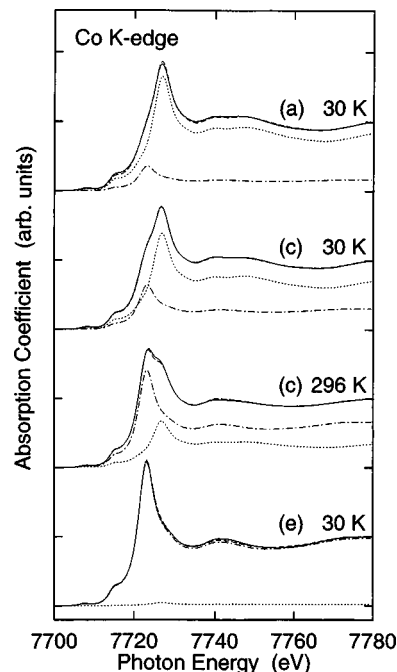


FIG. 5. Results of the factor analysis for the Co K -edge XANES spectra of samples (a) at 30 K, (c) at 30 and 296 K, and (e) at 30 K. Solid lines denote the experimental data, dotted lines the Co^{III} component, dot-dashed lines the Co^{II} components, and dashed lines the sum of the dotted and dot-dashed lines (fitted). The edge jumps for the Co^{II} and Co^{III} components are associated with the component ratios.

The obtained $\text{Co}^{\text{II}}/\text{Co}^{\text{III}}$ composition ratios are not always consistent with the results of the elemental analysis in Table I. If we assume the $\text{Co}^{\text{II}}/\text{Co}^{\text{III}}$ ratio by XANES and the Co:Fe ratio by the elemental analysis in sample (a), the maximum Rb composition (all Fe should be divalent) is estimated to be 0.45–0.46, which is smaller than that from the elemental analysis of 0.66 beyond the error. Such deviation can tentatively be understood by taking account of the fact that the present materials were obtained as a colloidal ultrafine powder and there should exist some alkali ions adsorbed on the charged surface.⁷ It should be noted that the bulk composition of Prussian blue analogs could be different from that estimated from the elemental analysis. For samples (b)–(f), no apparent contradictions were found between the XANES and elemental-analysis results; the maximum alkali compositions allowed were larger than those from the elemental analysis.

TABLE II. Co^{III} composition ratios $\text{Co}^{\text{III}}/[\text{Co}^{\text{II}}+\text{Co}^{\text{III}}]$ estimated from the Co K -edge XANES. The errors were roughly estimated to be a few percent for each composition ratio.

Sample	30 K	296 K
(a)	0.83	0.84
(b)	0.72	0.66
(c)	0.70	0.34
(d)	0.59	0.24
(e)	0.02	0.00
(f)	0.16	0.00

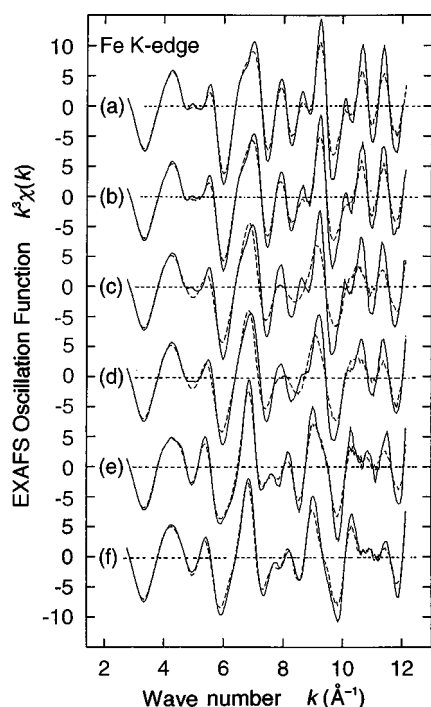


FIG. 6. Fe K -edge EXAFS oscillation functions $k^3\chi(k)$ of samples (a)–(f) taken at 30 K (solid lines) and 296 K (dashed lines).

V. EXAFS

A. Analysis of Fe-C and Fe-N shells in Fe K -edge EXAFS

The Fe K -edge EXAFS measurements were interrupted around $k = 12.3 \text{ \AA}^{-1}$ due to the presence of Co in all the samples. The EXAFS oscillation functions $k^3\chi(k)$ were obtained by means of standard analysis procedures: pre-edge base-line subtraction, postedge background estimation using the cubic spline function, and the normalization with the atomic absorption coefficients given in the literature.^{8,14} The resultant $k^3\chi(k)$ functions are depicted in Fig. 6, and corresponding Fourier transforms ($\Delta k_{\text{FT}} \cong 2.8\text{--}12.1 \text{ \AA}^{-1}$) are shown in Fig. 7. In Fig. 7, three dominant peaks were observed in all the spectra; the ones at 1.5, 2.5, and 4.4–4.8 \AA can be ascribed to the Fe-C, Fe-N, and Fe-Co shells, respectively. The latter two contributions are known to be subjected to the strong multiple-scattering effect because of the expected linear Fe-C-N-Co coordination.

The analysis of the Fe-C shell is straightforward because Fe^{II}-C and Fe^{III}-C distances are not different from each other and the one-shell fit can be applied. Although the Fe-N shell contains the multiple-scattering paths, all the Debye-Waller factors for the single (Fe-N-Fe), double (Fe-C-N-Fe or Fe-N-C-Fe), and triple (Fe-C-N-C-Fe) scattering paths are equal (if the dynamical effect of the scattering amplitude is neglected) since the Fe-C-N angles can be regarded as 180°. Note here that the Debye-Waller factors can be different between the reference and unknown samples. Thus the additive contributions of the multiple-scattering paths can be described with a single shell using the effective backscattering amplitude and phase shift, and the one-shell fit similar to the Fe-C shell is applicable for the Fe-N shell. The backscattering amplitudes and the phase shifts for the Fe-C and Fe-N shells were derived from the empirical standard of $\text{K}_3\text{Fe}^{\text{III}}(\text{CN})_6$ whose structure was determined by the x-ray-

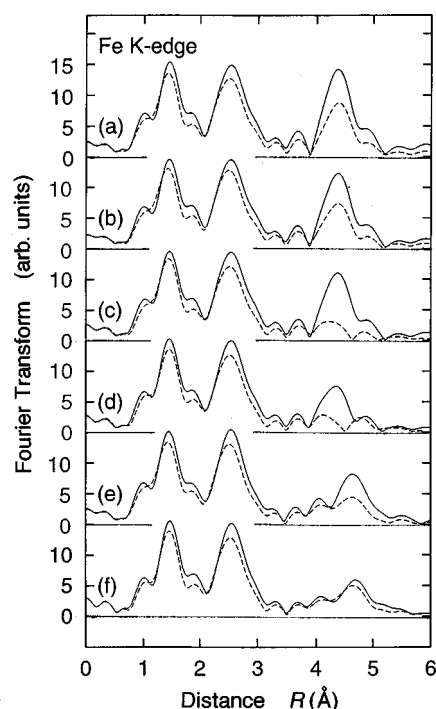


FIG. 7. Fourier transforms of Fe K -edge EXAFS oscillation functions $k^3\chi(k)$ (Fig. 6) of samples (a)–(f) taken at 30 K (solid lines) and 296 K (dashed lines).

diffraction analysis.¹⁵ In order to obtain the structure parameters of the coordination numbers and the interatomic distances, the curve-fitting analysis was performed in k space. The employed fitting ranges are summarized in Table III (analyses 1 and 2). The intrinsic reduction factor S_0^2 and the edge-energy shift ΔE_0 were assumed to be equal to those of the standard. The coordination number N , the interatomic distance R , and the mean-square relative displacement (the EXAFS Debye-Waller factor) C_2 were fitted. The results concerning N and R are summarized in Table IV.

B. Analysis of Co-N,O and Co-C shells in Co K -edge EXAFS

Co K -edge EXAFS oscillation functions $k^3\chi(k)$ were similarly extracted. Prior to the Co K -edge EXAFS analysis, several uncertainties should be verified and eliminated. First, there might be residual contribution of the Fe K -edge EXAFS in the Co K -edge EXAFS region. In order to check the effect, the EXAFS simulation using the FEFF6 code¹⁶ was carried out assuming the local structures of $\text{Fe}(\text{CN})_6\text{Co}_6$ and $\text{Co}(\text{NC})_6\text{Fe}_6$ for the Fe and Co K -edge EXAFS, respectively. Actually, a small contribution of the Fe K -edge EXAFS was found in the Co K -edge EXAFS region, although the three dominant peaks concerning Co-N, Co-C, and Co-Fe shells were not affected at all in their intensities or in their positions. The effect for the interatomic distances was also estimated. The deviations were found to be at most 0.003 \AA (the Co-C shell) when the Co K -edge EXAFS spectra were compared with and without the Fe K -edge EXAFS residuals. We will therefore hereafter neglect the Fe K -edge EXAFS residuals in the Co K -edge region.

Second, as indicated in Sec. III, there exists a small amount of Ni contaminations in all the samples. The obtained $k^3\chi(k)$ functions and corresponding Fourier trans-

TABLE III. Employed parameters in the EXAFS analysis. The Fourier-transform k range Δk_{FT} , the Fourier-filtered R range ΔR_{fit} , the curve-fitted k range Δk_{fit} are given. The fitting variables are N , R , C_2 in analyses 1 and 2; R , C_2 , C_3 in analyses 5, 12, and 16; and R , C_2 in all the other analyses.

Analysis No.	Sample No.	Δk_{FT} (\AA^{-1})	ΔR_{fit} (\AA)	Δk_{fit} (\AA^{-1})	Shell
Fe K edge					
1	(a)–(f)	2.8–12.1	0.8–1.8	4.0–11.5	Fe-C
2	(a)–(c)	2.8–12.1	2.0–3.2	4.0–11.5	Fe-N
3	(e), (f)	2.8–12.1	4.2–5.3	6.5–11.5	Fe-Co ^{II}
4	(a)–(d)	2.8–12.1	3.9–5.2	6.5–11.5	Fe-Co ^I , Fe-Co ^{III}
5	(a)–(d)	2.8–12.1	3.9–5.2	6.5–11.5	Fe-Co ^(av)
Co K edge					
6	(e), (f)	3.3–12.3	0.9–2.0	4.0–11.5	Co ^{II} -N,O
7	(e), (f)	3.3–12.3	2.0–3.4	4.0–11.5	Co ^{II} -C
8	(a) 30 K	2.8–16.0	1.05–1.95	4.0–15.0	Co ^{II} -N,O, Co ^{III} -N,O
9	(a) 30 K	2.8–16.0	1.95–3.30	4.0–15.0	Co ^{II} -C, Co ^{II} -C
10	(a), (b), (c) 30 K, (d) 30 K	2.8–12.3	1.1–3.2	4.0–11.5	Co ^{II} -N,O, Co ^{III} -N,O, Co ^{II} -C, Co ^{III} -C
11	(c) 296 K, (d) 296 K	3.5–12.1	1.1–3.2	4.0–11.5	Co ^{II} -N,O, Co ^{III} -N,O, Co ^{II} -C, Co ^{III} -C
12	(a), (b), (c) 30 K, (d) 30 K	2.8–12.3	1.1–3.2	4.0–11.5	Co ^(av) -N,O, Co ^(av) -C
13	(e), (f)	3.3–12.3	4.2–5.4	6.5–11.5	Co ^{II} -Fe
14	(a), (b), (c) 30 K, (d) 30 K	2.8–12.3	3.9–5.2	6.5–11.5	Co ^{III} -Fe, Co ^{II} -Fe
15	(c) 296 K, (d) 296 K	2.8–12.3	3.9–5.2	6.5–11.5	Co ^{III} -Fe, Co ^{II} -Fe
16	(a), (b), (c) 30 K, (d) 30 K	2.8–12.3	3.9–5.2	6.5–11.5	Co ^(av) -Fe

forms of sample (a) are shown in Figs. 8(a) and 8(b). These figures show reasonable contributions and indicate that the analysis can be performed over a sufficiently wide k range up to $\sim 15 \text{\AA}^{-1}$ where the Ni-K absorption might be less important because of stronger EXAFS oscillations. On the other hand, Fig. 8(c) shows the $k^3\chi(k)$ function of sample (c). Considerable contributions of Ni K -edge absorption can be seen at $k \sim 12.7 \text{\AA}^{-1}$; especially at 296 K the Ni K -edge absorption jump might be greater than the EXAFS oscillation. The amount of Ni contamination was estimated to be $\sim 0.1\%$ from the edge jump. In such a case, the analysis should be terminated at $k \sim 12.5 \text{\AA}^{-1}$.

In order to unify the assumed parameters through the Co K -edge EXAFS analysis, the employed maximum k ranges were restricted to $k \sim 12.3 \text{\AA}^{-1}$. The $k^3\chi(k)$ functions and their Fourier transforms are shown in Figs. 9 and 10, respectively. In Fig. 9, samples (c) and (d) exhibit noticeable temperature dependence, while the others are less temperature dependent, which is associated with amplitude dumpings at 296 K due to enhanced Debye-Waller factors. In Fig. 10, three dominant contributions are in principle observed for all the spectra; the ones at 1.5–1.8, 2.4–2.7, and 4.3–4.8 \AA can be assigned to the Co-N, O, Co-C, and Co-Fe shells. The first nearest-neighbor shell should contain both the Co-N and

TABLE IV. Analysis results of the Fe-C and Fe-N shells in the Fe K -edge EXAFS. Dominant Fe valences are also noted. The errors in N might be estimated to be $\sim 10\%$, while relative errors in $R(\text{Fe-C})$ and $R(\text{Fe-N})$ with respect to the standard should be 0.005 and 0.01 \AA , respectively.

Sample	T (K)	Fe valence	Fe-C		Fe-N	
			N	R (\AA)	N	R (\AA)
$\text{K}_3\text{Fe}^{\text{III}}(\text{CN})_6$	296	III	(6)	(1.940) ^a	(6)	(3.070) ^a
$\text{K}_4\text{Fe}^{\text{II}}(\text{CN})_6$	296	II	5.6	1.917	5.7	3.058
	(a) 30	II	6.4	1.911	5.8	3.035
(b)	296	II	6.3	1.915	5.8	3.043
	30	II	6.3	1.909	5.8	3.034
(c)	296	II	6.3	1.915	5.8	3.047
	30	II	6.3	1.915	5.8	3.039
(d)	296	III	6.3	1.931	5.8	3.046
	30	II	6.3	1.916	5.8	3.040
(e)	296	III	6.3	1.931	5.8	3.048
	30	II	6.3	1.908	5.8	3.039
(f)	296	II	6.3	1.915	5.8	3.051
	30	III	6.3	1.928	5.8	3.050
	296	III	6.3	1.933	5.8	3.052

^aReference 15.

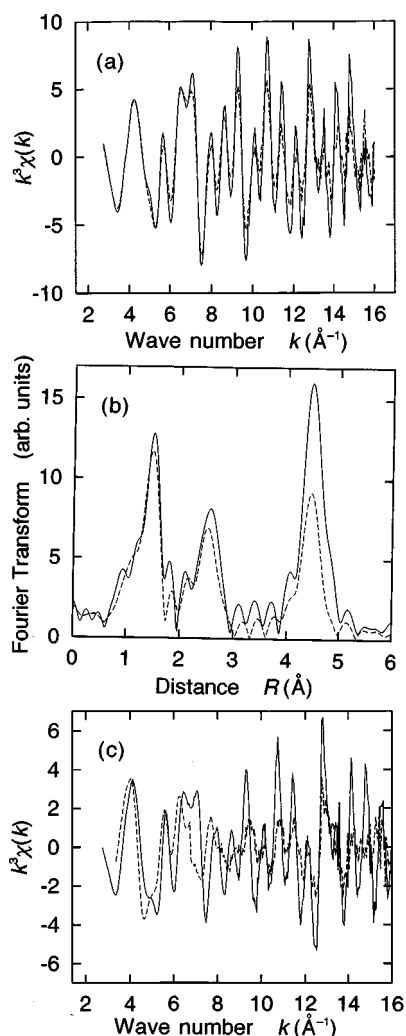


FIG. 8. (a) Co K -edge EXAFS oscillation functions $k^3\chi(k)$ of sample (a); (b) Fourier transforms of (a); (c) Co K -edge EXAFS oscillation function $k^3\chi(k)$ of sample (c). Solid lines correspond to the 30-K data, while dashed lines correspond to the 296-K data. Strong Ni K edges are found at $k \sim 12.7 \text{\AA}^{-1}$ in (c).

Co-O contributions, the latter of which originates from the H_2O coordination. The Fourier transforms of samples (a), (b), and (c) at 30 K, and sample (d) at 30 K resemble each other, implying that the dominant Co species are Co^{III} . On the other hand, those of samples (e) and (f) that contain almost exclusively Co^{II} species are similar to each other.

The analysis of the Co-N,O, and Co-C shells is much more complicated than the Fe K -edge case. Comparing the spectra of samples (a)–(d) with those of (e) and (f), the Co^{II} and Co^{III} species should provide considerably different EXAFS functions and thus multishell analyses should be performed. Moreover, in the Fourier transforms of samples (a)–(d), subpeaks located between the principle Co-N,O, and Co-C contributions were found to be ascribed to the superposition of the sidelobes of the two contributions. This implies that the Co-N, O, and Co-C shells cannot be separated in samples (a)–(d).

First of all, the analysis of samples (e) and (f) was performed. Since no suitable reference materials are available, the FEFF6 (Ref. 16) calculation was carried out to obtain the backscattering amplitudes and the phase shifts. Here we em-

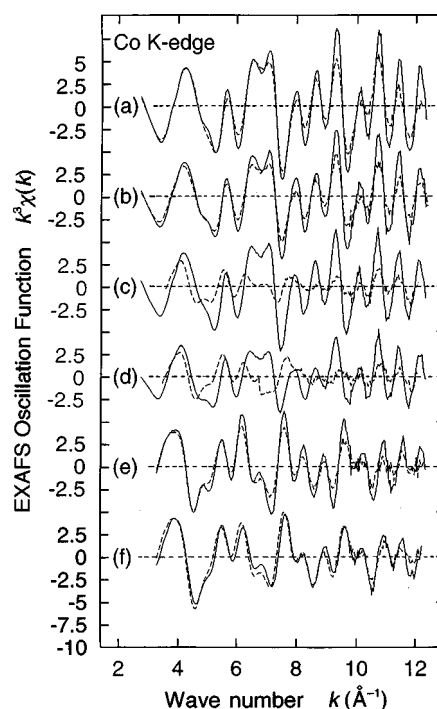


FIG. 9. Co K -edge EXAFS oscillation functions $k^3\chi(k)$ of samples (a)–(f) taken at 30 K (solid lines) and 296 K (dashed lines).

ployed an octahedral $\text{Co}(\text{NC})_6\text{Fe}_6$ cluster (the $\text{Co}^{\text{II}}\text{-N}$, $\text{Co}^{\text{II}}\text{-C}$, and $\text{Co}^{\text{II}}\text{-Fe}$ distances were assumed to be 2.08, 3.12, and 5.12 \AA , respectively). Here the two contributions of the $\text{Co}^{\text{II}}\text{-N,O}$ and $\text{Co}^{\text{II}}\text{-C}$ shells are well separated as seen in Fig. 10 and thus the one-shell fit was applicable to each shell. The employed k and R ranges are described in Table III (analyses 6 and 7). The first-nearest-neighbor shells contain both the

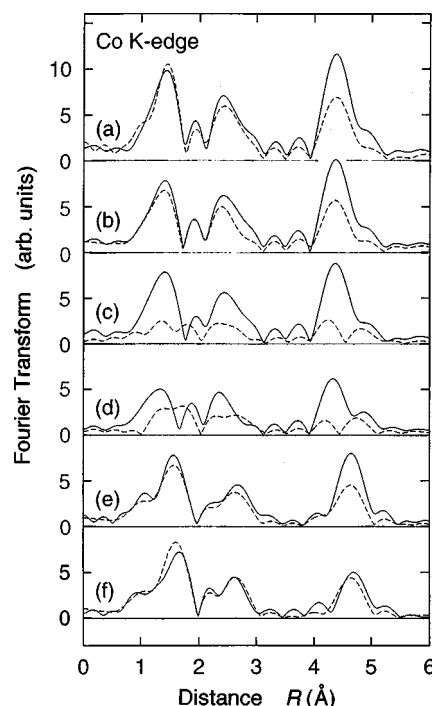


FIG. 10. Fourier transforms of Co K -edge EXAFS oscillation functions $k^3\chi(k)$ (Fig. 9) of samples (a)–(f) taken at 30 K (solid lines) and 296 K (dashed lines).

TABLE V. Employed S_0^2 and ΔE_0 for each shell (analyses 3–16 in Table III). The backscattering amplitudes and the phase shifts were derived from the theoretical standards FEFF6.

	Co ^{II} -N,O	Co ^{III} -N,O	Co ^{II} -C	Co ^{III} -C	Fe-Co ^{II}	Fe-Co ^{III}	Co ^{II} -Fe	Co ^{III} -Fe
S_0^2	0.71	0.71	1.00	1.00	0.66	0.66	0.39	0.39
ΔE_0	-1.5	-1.5	-1.5	-1.5	-4.4	-8.2	-5.5	-9.4

Co-N and Co-O contributions, while these shells are not distinguishable. Thus the first-nearest-neighbor shells were analyzed using only the Co-N parameters given by FEFF6. As given in Table V, we assumed $S_0^2=0.71$ and $\Delta E_0=-1.5$ eV for the Co^{II}-N,O shells and $S_0^2=1.00$ and $\Delta E_0=-1.5$ eV for the Co^{II}-C one. The values of S_0^2 and ΔE_0 were determined so that all the analysis for the Co-N,O and Co-C shells described below may provide appropriate fits. The expected N values also assumed as given in Table I, and only R and C_2 were optimized in the curve-fitting analysis. The results of the distances are summarized in Table VI.

Prior to the EXAFS analysis of samples (a)–(d), the spectrum of sample (a) at 30 K was analyzed using a wider k range as depicted in Figs. 8(a) and 8(b). Although a small amount of the Ni-K absorption is overlapped, the Co-N,O and Co-C shells were found to be separated well [Fig. 8(b)] and the analysis might be more reliable than that using a narrower k range. Nevertheless, since the Co^{II} and Co^{III} cations should show considerably different ionic radii, two-shell fits had to be performed for each contribution with the fitting ranges given in Table III (analyses 8 and 9). For the Co^{III}-N,O and Co^{III}-C EXAFS parameters, the FEFF6 calculation was carried out with the assumption of an octahedral Co(NC)₆Fe₆ cluster with the Co-N, Co-C, and Co-Fe distances of 2.08, 3.01, and 4.92 Å, respectively. The employed S_0^2 and ΔE_0 values are given in Table V, which were assumed to be equal to those of Co^{II}-N,O and Co^{II}-C ones. Since the Co^{II}:Co^{III} ratios were successfully given by the Co K -edge XANES spectra, the fitting variables should be R and C_2 (the number of fitting variables is four for the two-shell

fits). The distances were optimized to be $R(\text{Co}^{\text{II}}\text{-N,O})=2.085$ Å, $R(\text{Co}^{\text{III}}\text{-N,O})=1.892$ Å, $R(\text{Co}^{\text{II}}\text{-C})=3.205$ Å, and $R(\text{Co}^{\text{III}}\text{-C})=3.052$ Å.

Subsequently, the analysis using a narrower k range was carried out for sample (a) at 30 K (analyses 10 and 11 in Table III). Since the Co-N,O and Co-C shells are not separated, the four-shell fit for Co^{II}-N,O, Co^{III}-N,O, Co^{II}-C, and Co^{III}-C was conducted. The independent data point¹⁷ is $N_{\text{ind}}=2\Delta k_{\text{fit}}\Delta R_{\text{fit}}/\pi+1\cong 11$, which is larger than the number of fitting variables of eight (R and C_2 for each shell). The obtained distances, which are given in Table VI, are $R(\text{Co}^{\text{II}}\text{-N,O})=2.073$ Å, $R(\text{Co}^{\text{III}}\text{-N,O})=1.892$ Å, $R(\text{Co}^{\text{II}}\text{-C})=3.210$ Å, and $R(\text{Co}^{\text{III}}\text{-C})=3.053$ Å, which are all consistent with those obtained using a wider k range given above. The four-shell analysis using rather a narrow k range was thus justified. Similar analyses were subsequently carried out for samples (a)–(d) (analyses 10 and 11 in Table III). Moreover, in order to obtain the average Co^(av)-N,O and Co^(av)-C distances, the two-shell fits were also performed (analysis 12 in Table III). The assumed parameters such as the backscattering amplitudes, the phase shifts, S_0^2 , and ΔE_0 were the ones for Co^{III}-N,O and Co^{III}-C shells. Here for the description of asymmetric distribution due to two kinds of shells (Co^{II}-N,O and Co^{III}-N,O) the mean cubic relative displacement C_3 was added as a fitting variable. The consequent distances were also summarized in Table VI. No good fitting results for the average distances were obtained for sample (c) or (d) at 296 K.

C. Analysis of Fe-Co shells in Fe and Co K -edge EXAFS

As found in the Fourier transforms shown in Figs. 7 and 10, the Fe-Co shells were observed for all the materials. Al-

TABLE VI. Obtained interatomic distances R of the Co-N, O and Co-C shells in the Co K -edge EXAFS. For samples (a)–(d), the Co^{III} ratios given by the XANES analysis were used, while for (e) and (f) the Co^{III} components were assumed to be absent. The relative errors might be at most 0.01–0.02 Å. The values in parentheses are just algebraic averages since the one-shell analyses failed.

Sample	T (K)	Co ^{III} ratio	$R(\text{Co-N,O})$ (Å)			Co ^{III}	$R(\text{Co-C})$ (Å)	
			Co ^{III}	Co ^{II}	Average		Co ^{II}	Average
(a)	30	0.83	1.892	2.073	1.920	3.053	3.210	3.095
	296	0.84	1.902	2.070	1.933	3.050	3.208	3.084
(b)	30	0.72	1.894	2.079	1.943	3.050	3.196	3.106
	296	0.66	1.900	2.094	1.954	3.046	3.201	3.118
(c)	30	0.70	1.890	2.048	1.941	3.049	3.188	3.096
	296	0.34	1.929	2.113	(2.049)	3.064	3.227	(3.170)
(d)	30	0.59	1.910	2.111	2.009	3.055	3.211	3.153
	296	0.24	1.962	2.121	(2.083)	3.068	3.239	(3.198)
(e)	30	0.00		2.081	2.081		3.250	3.250
	296	0.00		2.102	2.102		3.260	3.260
(f)	30	0.00		2.095	2.095		3.213	3.213
	296	0.00		2.110	2.110		3.243	3.243

TABLE VII. Obtained Fe-Co distances from the Fe [$R(\text{Fe-Co})$] and Co [$R(\text{Co-Fe})$] K -edge EXAFs. For samples (a)–(d), the Co^{III} ratios given by the XANES analysis were used, while for (e) and (f) the Co^{III} components were assumed to be absent. The relative and absolute errors might be ~ 0.03 and ~ 0.06 Å, respectively. The values in parentheses are just algebraic averages since the one-shell analyses failed. Half values of the lattice constants a_0 are also given for comparison.

Sample	$T(\text{K})$	Co^{III} ratio	$R(\text{Fe-Co})$ (Å)			$R(\text{Co-Fe})$ (Å)			$a_0/2$ (Å)
			Co^{III}	Co^{II}	Average	Co^{III}	Co^{II}	Average	
(a)	30	0.83	4.94	5.13	4.97	4.97	5.21	5.00	4.98
	296	0.84	4.94	5.14	4.98	4.98	5.22	5.00	
(b)	30	0.72	4.94	5.12	4.98	4.97	5.19	5.01	4.98
	296	0.66	4.95	5.14	5.00	4.98	5.20	5.01	
(c)	30	0.70	4.95	5.13	4.99	4.98	5.20	5.01	5.17
	296	0.34	4.98	5.18	(5.11)	4.98	5.20	(5.12)	
(d)	30	0.59	4.95	5.15	5.02	4.96	5.20	5.03	5.16
	296	0.24	4.97	5.17	(5.12)	4.96	5.19	(5.13)	
(e)	30	0.00		5.18	5.18		5.20	5.20	5.16
	296	0.00		5.19	5.19		5.20	5.20	
(f)	30	0.00		5.16	5.16		5.19	5.19	5.16
	296	0.00		5.17	5.17		5.20	5.20	

though the shells are subjected to the strong multiple-scattering effect due to the collinear arrangement of the Fe-C-N-Co unit, similar analyses to those for the Fe-N and Co-C shells can be performed. The backscattering amplitudes and the phase shifts for the Fe- Co^{II} and Fe- Co^{III} shells were obtained by the FEFF6 calculations for octahedral $\text{Fe}(\text{CN})_6\text{Co}_6$ clusters, the interatomic distances being assumed to be the same as those for $\text{Co}(\text{NC})_6\text{Fe}_6$ described above. For the Co^{II} -Fe and Co^{III} -Fe shells, the above FEFF results were employed. The detailed analysis parameters are given in Tables III and V. The two-shell fittings were performed to obtain the distances for the Fe- Co^{II} and Fe- Co^{III} shells or the Co^{II} -Fe and Co^{III} -Fe ones, while the one-shell fittings were also carried out to provide the average distances of Fe- $\text{Co}^{\text{(av)}}$ and $\text{Co}^{\text{(av)}}$ -Fe shells. The $\text{Co}^{\text{II}}:\text{Co}^{\text{III}}$ ratios for samples (a)–(d) were assumed to the ones given by Co K -edge XANES, while the Co^{III} components were neglected in samples (e) and (f). The consequently obtained Fe-Co and Co-Fe distances are summarized in Table VII.

D. Discussion

From the Fe K -edge EXAFS analysis for the Fe-C and Fe-N shells, it is confirmed that the local structure around Fe is $\text{Fe}(\text{CN})_6$ in all the materials. Moreover, the Fe^{III} -C distances are found to be slightly longer than the Fe^{II} -C distance, though the differences are within the errors. Although usually higher-valent cations should exhibit shorter metal-ligand bond distances due to a smaller ionic radius, the present results are not the case, including the reference materials of $\text{K}_3\text{Fe}^{\text{III}}(\text{CN})_6$ and $\text{K}_4\text{Fe}^{\text{II}}(\text{CN})_6$. This can be explained by the nature of the Fe and CN^- chemical bonds. In the bondings between transition-metal cations and CN^- , the π bond concerning the metal $3dt_{2g}$ and the $\text{CN} \pi^*$ levels plays an important role. The lack of one bonding electron in the Fe $3dt_{2g}$ level for $\text{Fe}^{\text{III}}(\text{CN})_6^{3-}$ results in a slight elongation of the Fe-C distance compared to the case of $\text{Fe}^{\text{II}}(\text{CN})_6^{4-}$.

On the other hand, the difference between the Co^{II} -N,O and Co^{III} -N,O distances given in Table VI is more signifi-

cant. The Co^{II} -N,O and Co^{III} -N,O distances are distributed in the ranges of 2.048–2.121 and 1.890–1.962 Å, respectively, the differences being as much as 0.16–0.20 Å. This mainly causes the differences in the lattice constants a_0 given in Table I. The distance difference of 0.158–0.201 Å is larger than that for typical Co^{II} spin-crossover complexes (0.09–0.13 Å) and is comparable with that for Co tautomeric complexes (0.16–0.22 Å). These findings are quite reasonable since the present materials show the changes of Co valences essentially similar to the cases of tautomeric complexes. In the Co^{II} high-spin state, two electrons are present at the σ -antibonding $3de_g$ levels, leading to significant elongation of the Co-ligand bonds compared to that in the Co^{III} low-spin state where no electrons occupy the $3de_g$ levels.

As shown in Table VII, the Fe-Co distances are in fairly good agreement with the Co-Fe distances, although the latter were estimated slightly longer. The average Fe-Co (Co-Fe) distances are very consistent with the values of one half of the lattice constant a_0 , indicating reliability of the present analyses and the collinear arrangement of the Fe-C-N-Co unit.

VI. CONCLUSION

Fe and Co K -edge x-ray-absorption fine-structure spectra were measured and analyzed for several FeCo cyanides $M_x\text{Co}_y\text{Fe}(\text{CN})_6 \cdot z\text{H}_2\text{O}$ ($M = \text{Na}, \text{K}, \text{Rb}$). The $\text{Co}^{\text{II}}:\text{Co}^{\text{III}}$ ratios were successfully determined from the Co K -edge XANES spectral analysis. Such an application of XANES can be performed for various kinds of materials and should be emphasized in a methodological sense. It was found that the content of alkali ions (Rb^+) does not always provide the bulk concentration possibly because of a significant amount of adsorbed ions on the ultrafine powders. The local structures around Fe and Co atoms were determined by Fe and Co K -edge EXAFS. It is confirmed that the local structures around Fe are $\text{Fe}(\text{CN})_6\text{Co}_6$ while those around Co are $\text{Co}(\text{NC})_{6-1/y}(\text{H}_2\text{O})_{1/y}\text{Fe}_{6-1/y}$. The Fe-C distances were found to be almost constant (1.91–1.93 Å) for all the

samples, while the Co-N,O distances vary significantly depending on the Co valence. The observed change of the lattice constants can be ascribed to the variation of the local structure around Co. The present findings are very useful to the understanding of the magnetic properties of these materials.

ACKNOWLEDGMENTS

The authors gratefully acknowledge S. Terada and Y. Einaga of The University of Tokyo for their help in the XAFS measurements. The present work has been performed under the approval of Photon Factory Program Advisory Committee (PF-PAC No. 97G034).

-
- ¹T. Mallah, S. Thiebaut, M. Verdaguer, and P. Veillet, *Science* **262**, 1554 (1993).
²R. E. William and G. S. Girolami, *Science* **268**, 397 (1995).
³S. Ferlay, T. Mallah, R. Ouahés, P. Veillet, and M. Verdaguer, *Nature (London)* **378**, 701 (1995).
⁴O. Sato, T. Iyoda, A. Fujishima, and K. Hashimoto, *Science* **271**, 49 (1996).
⁵O. Sato, T. Iyoda, A. Fujishima, and K. Hashimoto, *Science* **272**, 704 (1996).
⁶S. Ohkoshi, T. Iyoda, A. Fujishima, and K. Hashimoto, *Phys. Rev. B* **56**, 11 642 (1997).
⁷H. J. Buser, D. Schwarzenbach, W. Peter, and A. Ludi, *Inorg. Chem.* **16**, 2704 (1977).
⁸See, for instance, *X-ray Absorption: Principles, Applications, Techniques of EXAFS, SEXAFS and XANES*, edited by D. C. Koningsberger and R. Prins (Wiley, New York, 1988).
⁹O. Sato, Y. Einaga, T. Iyoda, A. Fujishima, and K. Hashimoto, *J. Phys. Chem. B* **101**, 3903 (1997).
¹⁰O. Sato, Y. Einaga, and K. Hashimoto (unpublished).
¹¹M. Nomura (unpublished); M. Nomura and A. Koyama (unpublished).
¹²N. Kosugi, T. Yokoyama, and H. Kuroda, *Chem. Phys.* **104**, 449 (1986).
¹³M. Fernández-García, C. Márquez Alvarez, and G. L. Haller, *J. Phys. Chem.* **99**, 12 565 (1995).
¹⁴T. Yokoyama, H. Hamamatsu, and T. Ohta, computer code EXAFSH, Version 2.1, The University of Tokyo, 1993.
¹⁵B. N. Figgis, M. Gerloch, and R. Mason, *Proc. R. Soc. London, Ser. B* **309**, 91 (1969).
¹⁶S. I. Zabinsky, J. J. Rehr, A. Ankudinov, R. C. Albers, and M. J. Eller, *Phys. Rev. B* **52**, 2995 (1995).
¹⁷*Report of the International Workshop on Standards and Criteria in X-ray Absorption Spectroscopy*, edited by J. Mustre de León, E. A. Stern, D. E. Sayers, Y.-J. Ma, and J. J. Rehr [*Physica B* **158**, 701 (1989)].